Dalton Transactions

ROYAL SOCIETY OF CHEMISTRY

COMMUNICATION

View Article Online
View Journal | View Issue

Cite this: *Dalton Trans.*, 2026, **55**, 3667

Received 7th January 2026,
Accepted 28th January 2026

DOI: 10.1039/d6dt00038j

rsc.li/dalton

Synthesis, characterisation and biological properties of a silver helicate which displays enhanced activity towards methicillin-resistant *Staphylococcus aureus* (MRSA)

Peltine Ndifon,[a] Emma C. Pinder,[a] Christopher H. L. Slater,[a] Christopher J. Clemett,[a] Auska A. T. McRobbie,[a] Samuel P. Rayner,[a] Shalith Wickramarachchi,[a] Karima Bertal-Ngaage,[a] Simon J. Allison,[a] Rebecca Dowey,[a] Jane Harmer,[a] Martin Carr,[a] Anthony J. Slate,[a] Roger M. Phillips,[a] Jonathan A. Butler,[b] Craig R. Rice [a] and Martina Whitehead *[a]

Antimicrobial resistance is an ever growing concern and the development of novel treatment methods is urgently required. In this study a novel bis-bidentate ligand strand which forms a dinuclear double helicate in solution with silver cations, $[Ag_2L_2]^{2+}$ demonstrated cytotoxicity against a range of cancer cell lines and antimicrobial activity against bacterial pathogens *E. coli*, *P. aeruginosa* and *S. aureus* (a methicillin resistant strain; MRSA), with the latter being at least 8 times more sensitive to the helicate complex compared to silver cations on their own.

The study of self-assembled systems with ligand strands and metal ions has become a significant area of research and the ability to produce discrete architectures containing multiple metal ions and ligands is now well established.[1–5] One area of study that has emerged from this field of interest is the investigation of metallosupramolecular systems for potential therapeutic applications.[6–10] Hannon *et al.*, has demonstrated that an Fe(II)-containing dinuclear triple helicate (*e.g.* $[L_3Fe_2]^{4+}$) interacts strongly with duplex DNA and displays both anticancer and anti-bacterial properties.[11,12] Scott and co-workers demonstrated that Fe(II)-containing "head-to-head-to-tail" helicates show selective *in vitro* cytotoxic activity against a range of cancer cell lines with IC_{50} values comparable to *cis*-platin.[13,14] Ruthenium containing transition metal helicates and mesocates have also been shown to have interesting biological properties with some showing higher cytotoxicity towards cancer cells that lack p53, a key tumour suppressor protein.[15] Metallacycles and metallacages have also been shown to possess useful properties with Casini *et al.*, reporting $[Pd_2L_4]^{4+}$ cages which demonstrated cytotoxicity towards an array of different human cancer cell lines.[16] Whilst silver-containing self-assemblies are well known, their potential anti-cancer and anti-microbial agent activity has, apart from a few noticeable exceptions, been relatively less well studied.[17–22] This is somewhat surprising as monocationic silver is a classic antimicrobial agent, yet studies of its supramolecular assemblies have only shown activity against methicillin resistant *Staphylococcus aureus* (MRSA) similar to that of the native cation.[18] The investigation of the antibacterial properties of silver complexes is an important area of study as the over-use of simple silver salts (*e.g.* $AgNO_3$) has led to an increase in silver resistance in bacteria such as *Pseudomonas aeruginosa*, *Escherichia coli* and *Staphylococcus aureus* (MRSA). All of these pathogens have been designated as critical priority pathogens by the World Health Organisation (WHO), due to their high threat to public health characterised by their resistance to multiple antibacterials (ESKAPEE pathogens).[23,24] In this work we demonstrate a bis-bidentate ligand strand which forms a dinuclear double helicate in solution with silver cations, $[Ag_2L_2]^{2+}$, that is toxic towards a panel of human cancer cell lines with IC_{50} values in the low to mid μM range and is selective to some cancer cell lines. It also displays antimicrobial activity against bacterial pathogens *E. coli*, *P. aeruginosa* and *S. aureus*, with the latter being at least 8 times more sensitive to the helicate complex compared to silver cations on their own. This study demonstrates the vast potential of supramolecular chemistry, more specifically silver helicates, in both cancer and antimicrobial therapeutics (Fig. 1).

The ligand **L** contains two bidentate binding domains arising from pyridyl-thiazole and a pyridyl-pyrazolyl N-donor units, bridged by a 1,3-tolyl spacer. Reaction of this ligand with AgOTf in MeCN gave a colourless solution from which colourless crystals were deposited upon slow diffusion of diisopropyl ether. Analysis of the crystal by X-ray diffraction showed that in the solid-state each ligand coordinates a silver metal

[a]*Department of Physical and Life Sciences, School of Applied Sciences, University of Huddersfield, Huddersfield, HD1 3DH, UK. E-mail: m.whitehead@hud.ac.uk*
[b]*Faculty of Science and Engineering, Manchester Metropolitan University, Manchester, M1 5GD, UK*

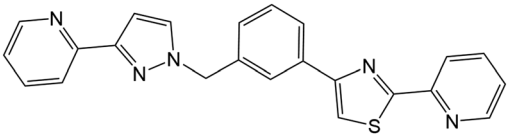

Fig. 1 Bis-bidentate pyridyl-thiazole and pyridyl-pyrazolyl containing ligand **L**.

ion *via* both terminal bidentate units separated by the 1,3-tolyl spacer. The silver metal ion's 4-coordinate geometry is completed by coordination of a different ligand to each metal ion, which itself coordinates another $[Ag\mathbf{L}]^+$ unit to give a chain of repeating ligand–metal units $\{[Ag\mathbf{L}]^+\}_\infty$. The Ag–N bond lengths range from 2.2193 (16)–2.4683 (15) Å and the N–Ag–N bond angles ranging from 153.74 (6) to 71.93 (5)° with a τ'_4 value ~0.48 (where $\tau'_4 = 1$ is perfectly tetrahedral whereas $\tau'_4 = 0$ is square planar).[23,25] Interestingly, each of the Ag^+ ions are coordinated *via* both a bidentate pyridyl-thiazole and pyridyl-pyrazolyl unit and due to the unsymmetrical nature of the ligand these can be thought of as a "head" and a "tail" and as each metal ion is coordinated *via* both units it can be considered a *head-to-tail* helicate polymer $\{[Ag\mathbf{L}](OTf)\}_\infty$ (Fig. 2).

Reaction of the same ligand with $AgClO_4$ in MeCN again gives colourless crystals upon diffusion of diethyl ether. However, in this case a *head-to-tail* dinuclear double helicate results. In the crystal each silver metal ion has 4-coordinate geometry formed from coordination of both a pyridyl-thiazole and pyridyl-pyrazolyl units with the geometry completed by coordination by a different ligand. The Ag–N bond lengths range from 2.239 (2)–2.5356 (18) Å and the N–Ag–N bond angles ranging from 153.74 (6) to 71.93 (5)° with a τ'_4 value ~0.47 very similar to that observed in the polymeric structure.[23,25] However, unlike the previous structure this additional ligand does not coordinate with a different $[Ag\mathbf{L}]^+$ subunit but rather it coordinates both metal ions within the same molecule with the '*over-and-under*' ligand motif requisite of helical chirality. Again, each metal ion is coordinated by both a bidentate pyridyl-thiazole and pyridyl-pyrazolyl unit resulting in a *head-to-tail* dinuclear double helicate (Fig. 3).

Solution state analysis of isolated $\{[Ag\mathbf{L}](OTf)\}_\infty$ (CD_3CN) shows both the expected 15 aromatic signals and a singlet at 5.06 ppm (corresponding to the methylene unit), in good agreement to the structure observed in the solid-state. The same is observed for isolated $[Ag_2\mathbf{L}_2](ClO_4)_2$ although the signals are shifted when compared to the triflate analogue. However, despite the difference in chemical shift it is not attributed to two different species as analysis of a mixture of both the isolated materials $\{[Ag\mathbf{L}](OTf)\}_\infty$ and $\{[Ag\mathbf{L}](OTf)\}_\infty$ in CD_3CN gives a ^1H NMR spectrum containing a single species (as opposed to two different species *e.g.*, polymer and double helicate). Rather we attribute this difference in chemical shift to the amount of water present in the solvent, as addition of a small amount of D_2O to the "mixed" NMR sample results in a change of the chemical shift. Upon addition of deuterium oxide, the ^1H NMR now more resembles that obtained for $[Ag_2\mathbf{L}_2](ClO_4)_2$ which is not surprising as perchlorate salts (and indeed $AgClO_4$ itself) are substantially more hygroscopic than the triflate analogues. ESI-MS analysis shows remarkably similar spectrum for both species with ions at *m*/*z* 1155 and 1105 corresponding to $\{[Ag_2\mathbf{L}_2](OTf)\}^+$ and $\{[Ag_2\mathbf{L}_2](ClO_4)\}^+$ respectively as well as *m*/*z* 502 ($\{(Ag\mathbf{L})^+\}$). As a result of this data, it would seem likely that in solution the dinuclear double helicate predominates and the formation of the polymer is an artifact of the crystallisation process and is only observed in the solid-state (Fig. 4).

To investigate whether these novel silver helicates have any cytotoxic activity against cancer cells *in vitro*, chemosensitivity studies were performed. However, this was limited to the $[Ag_2\ \mathbf{L}_2](OTf)_2$ complex as perchlorate anions are toxic to biological systems as they cannot be differentiated from iodide, and in humans they would interfere with iodide uptake by the thyroid.[26]

Human cancer cell lines derived from several different cancer tissue types were tested; colorectal carcinoma (HCT116), triple-negative breast cancer (MDAMB-231, HCC1937) and pancreatic

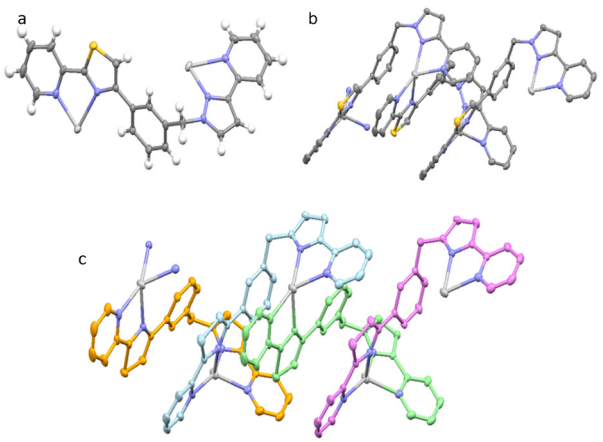

Fig. 2 Three views of the X-ray structure of $\{[Ag\mathbf{L}](OTf)\}_\infty$. Thermal ellipsoids shown at the 30% probability level. Remaining anions are omitted for clarity. Fig 2a and 2b colour code: silver, Ag(I); blue, N; yellow, S; white H; grey, C, (2c the ligand strands have been coloured for clarity).

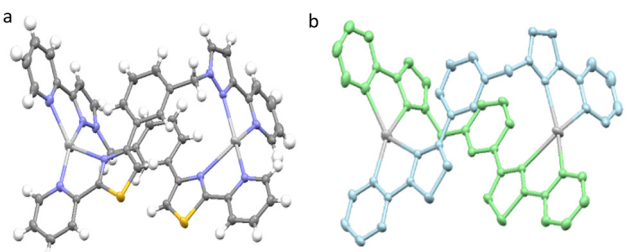

Fig. 3 Two views of the X-ray structure of $[Ag_2L_2](ClO_4)_2$. Thermal ellipsoids shown at the 30% probability level. Remaining anions are omitted for clarity. Fig 3a colour code: silver, Ag(I); blue, N; yellow, S; white H; grey, C, (3b the ligand strands have been coloured for clarity).

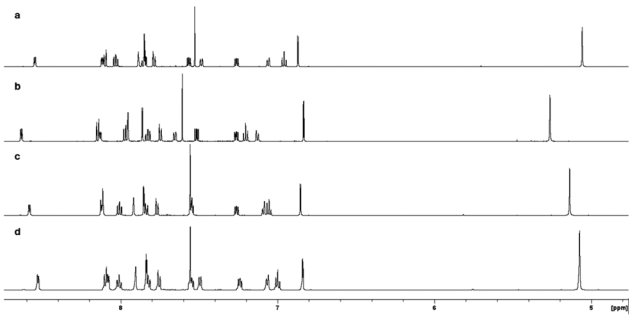

Fig. 4 Selected regions of the ^{1}H NMR (CD_3CN) of (a) $[Ag_2L_2](ClO_4)_2$, (b) $[Ag_2L_2](OTf)_2$, (c) mixture of isolated $[Ag_2L_2](ClO_4)_2$ and $[Ag_2L_2](OTf)_2$ and (d) $[Ag_2L_2](ClO_4)_2$ and $[Ag_2L_2](OTf)_2$ plus 50 μL D_2O.

cancer (PSN-1) and compared to a non-cancerous retinal epithelial cell line as a control (ARPE-19) (Fig. 5). For all of the tested cell lines, cytotoxicity of $[Ag_2\mathbf{L}_2](OTf)_2$ was in the low- to mid-micromolar range and was most active against the human pancreatic cancer cell line PSN-1 (IC_{50} of 1.51 μM). Whilst $[Ag_2\mathbf{L}_2](OTf)_2$ showed similar activity against the two triple-negative breast cancer cell lines as against confluent ARPE-19 retinal epithelial non-cancer cells, $[Ag_2\mathbf{L}_2](OTf)_2$ was preferentially cytotoxic against both the colorectal carcinoma cell line HCT116 (by ~2.7×) and against PSN-1 pancreatic cancer cells (~3.5× more active than against the non-cancer cells).

Metallosupramolecular chemistry shows great potential in the development of therapeutics for the treatment of antimicrobial resistant bacteria. In this study, the minimum inhibitory concentration (MIC) and minimum bactericidal concentration (MBC) of the silver helicate $[Ag_2\mathbf{L}_2]^{2+}$ was determined against *E. coli* (CFT073), *P. aeruginosa* (PAO1-LAC) and *S. aureus* (NCTC 12493; a methicillin resistant *S. aureus* (MRSA) strain) (Table 1). Against Gram-negative *E. Coli*, a two-

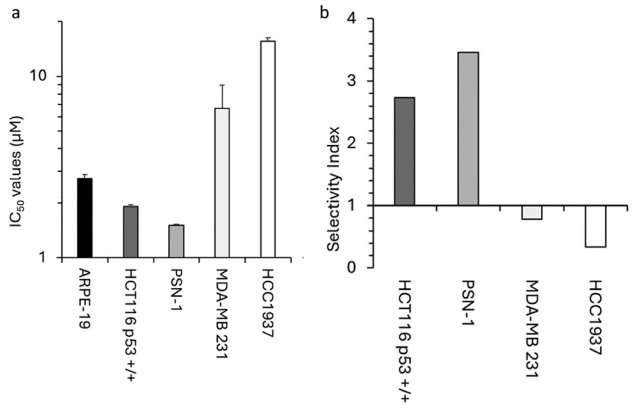

Fig. 5 Response of human cancer cell lines HCT116, PSN-1, MDA-MB-231 and HCC1937 and of non-cancerous ARPE-19 cells to $[Ag_2L_2](OTf)_2$ following 96 h continuous exposure. (a) The results presented represent the mean IC_{50} ± SD from three independent biological experiments. (b) Cancer selectivity index *in vitro* as determined by dividing the mean IC_{50} of ARPE-19 cells by the mean IC_{50} for $[Ag_2L_2](OTf)_2$ against cancer cell lines. A selectivity index >1 indicates fold preferential cytotoxicity towards the tested cancer cells (n = 3).

Table 1 Minimum Inhibitory Concentration (MIC) and Minimum Bactericidal Concentration (MBC) of silver triflate, $[Ag_2L_2](OTf)_2$ and free ligand against *Escherichia coli*, *Pseudomonas aeruginosa* and *Staphylococcus aureus*. DMSO was included as a solvent control. For the concentration calculation, the molecular weight of [AgL](OTf) was used so that the amount of silver cations in the complex and AgOTf is equimolar. Using the molecular weight of $[Ag_2L_2](OTf)_2$ the MIC for the complex is estimated to be half of that reported (n = 3). Ligand **L** showed MIC/MBC > 1000 μM and DMSO solvent control MIC/MBC > 5% (n = 3)

		$[Ag_2\mathbf{L}_2]^{2+}$	AgOTf
E. coli (CFT073)	MIC (μM)	15.6	31.25
	MBC (μM)	15.6	31.25
P. aeruginosa (PAO-LAC)	MIC (μM)	15.6–31.25	31.25
	MBC (μM)	31.25	31.25
S. aureus (NCTC 12493)	MIC (μM)	15.6	125
	MBC (μM)	15.6	125–250

fold decrease in both the MIC and MBC were observed with the silver complex (15.6 μM) compared to the silver triflate analogue (31.25 μM), whilst against *P. aeruginosa* MIC/MBCs were similar for both compounds ($[Ag_2\mathbf{L}_2]^{2+}$: 15.6–31.25 μM and silver triflate: 31.25 μM). Interestingly however the utilisation of $[Ag_2\mathbf{L}_2]^{2+}$ against MRSA dramatically reduced the MIC from 125 μM to 15.6 μM, when compared to the silver triflate analogue. This indicates that against MRSA (a Gram-positive species) the silver complex demonstrated a more potent antimicrobial activity than the native silver cations alone. This is interesting as silver-based antimicrobial compounds traditionally show enhanced antimicrobial activity against Gram-negative bacterial species (compared to that of Gram-positive) and this is thought to originate from the differences in cell wall structure; Gram positive bacterial species have a thick layer of peptidoglycan (which can hinder the penetration of silver ions) whilst Gram negative species have a thin layer of peptidoglycan that is encased in an outer membrane which is decorated with lipopolysaccharides, this outer membrane also consists of specific outer membranes that can facilitate silver entry.[27,28] Future studies will look to explore the mechanistic nature of this silver complex to further elucidate the enhanced antimicrobial activity against the MRSA strain.

Scanning electron microscopy (SEM) analysis of treated MRSA cells was performed to visualise complex mediated effects on bacterial morphology and cellular ultrastructure. At MIC and MBC concentrations of complex (15.6 μM), MRSA exhibited phenotypic changes to the classical coccoidal shape (Fig. 6C) compared to untreated (Fig. 6A) and DMSO (5%) treated solvent controls (Fig. 6B). At above the MBC (31.25 μM), visible concavities and pits were observed within the MRSA cells (Fig. 6D) suggesting a loss of structural integrity in response to the complex. At twice the MBC (62.5 μM) of the complex against MRSA, similar cell pitting was observed coupled with an uneven appearance within the ultrastructure (Fig. 6E), which was comparable to that observed at high concentrations (250 μM and 500 μM) of Ag^+ alone (Fig. 6F and G).

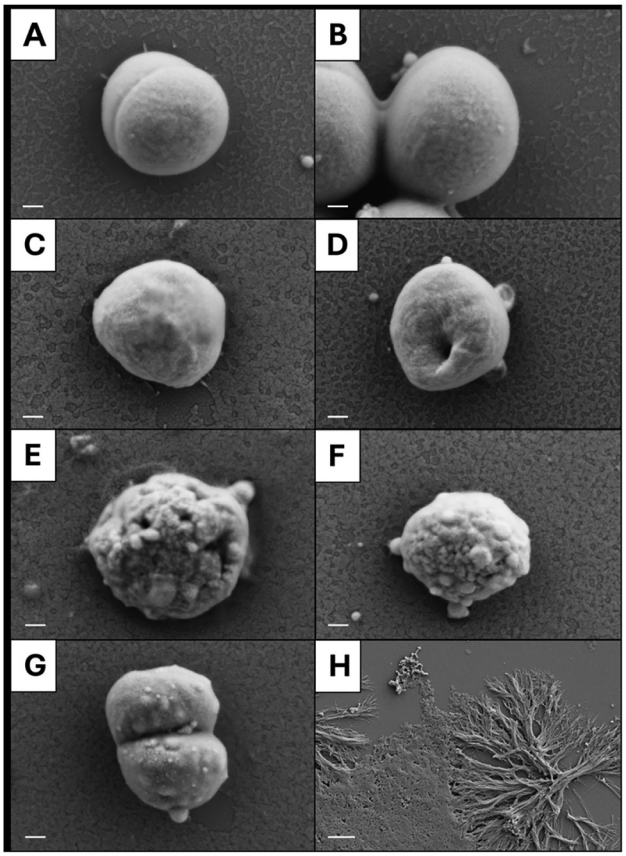

Fig. 6 Scanning electron micrographs of *S. aureus* (NCTC 12493; a methicillin resistant *S. aureus* (MRSA) strain). (A) without complex and after 24 h treatment with (B) DMSO (5%), (C) 15.625 μM [Ag**L**](OTf), (D) 31.25 μM [Ag**L**](OTf), (E) 62.5 μM [Ag**L**](OTf), (F) 250 μM Ag(OTf), (G) 500 μM Ag(OTf) and (H) 1 mM [Ag**L**](OTf) without bacterial cells. Scale bars denote 100 nm at magnification of ×75 000 (A–G) and 1 μm at ×10 000 (H).

In this study, we have demonstrated how a self-assembled dinuclear double silver helicate is toxic towards cancer cell lines and shows *in vitro* selectivity towards colorectal and pancreatic cancer cell lines relative to epithelial non-cancer cells. Furthermore, the complex $[Ag_2\mathbf{L}_2](OTf)_2$ is toxic towards the three bacterial strains tested, displaying similar or greater toxicity than AgOTf. Notably, in the case of the methicillin resistant *S. aureus* (MRSA) strain, which displays enhanced resistance towards AgOTf (MIC = 125 μM) the complex $[Ag_2\mathbf{L}_2](OTf)_2$ demonstrated enhanced antimicrobial properties (MIC and MBC = 15.6 μM). The threat to health due to the increase in antimicrobial resistance is of great concern and a major challenge to society, and this study clearly demonstrates that metallosupramolecular systems can play an essential part in the development of novel antimicrobial agents.

Conflicts of interest

The authors have no conflicts of interest to declare.

Data availability

The data supporting this article have been included as part of the supplementary information (SI). Supplementary information is available. See DOI: https://doi.org/10.1039/d6dt00038j.

CCDC 2516767 ($[Ag_2\mathbf{L}_2](ClO_4)_2{\cdot}0.5Et_2O{\cdot}0.5MeCN$) and 2516768 ($[\{[Ag\mathbf{L}](OTf)\}_\infty]$) contain the supplementary crystallographic data for this paper.[29a,b]

Acknowledgements

The authors would like to thank the Core Facilities Team at the Faculty of Science and Engineering, Manchester Metropolitan University, more specifically Dr Yibing Zhu for assistance with Scanning Electron Microscopy.

References

1 J.- M. Lehn, *Science*, 1993, **260**, 1762–1723.
2 J.-M. Lehn, *Angew. Chem., Int. Ed. Engl.*, 1990, **29**, 1304–1319.
3 J. W. Steed and J. L. Atwood, *Supramolecular Chemistry*, John Wiley and Sons, Chichester, 2000.
4 M. J. Hannon and L. J. Childs, *Supramol. Chem.*, 2004, **16**, 7–22.
5 C. Piguet, G. Bernardinelli and G. Hopfgartner, *Chem. Rev.*, 1997, **97**, 2005–2062.
6 A. Ahmedova, *Front. Chem.*, 2018, **6**, 620.
7 T. R. Cook, V. Vajpayee, M. H. Lee, P. J. Stang and K.-W. Chi, *Acc. Chem. Res.*, 2013, **46**, 2464–2474.
8 R. A. Kaner and P. Scott, *Future Med. Chem.*, 2015, **7**, 1–4.
9 K. Nisa, I. A. Lone, W. Arif, P. Singh, S. U. Rehmen and R. Kumar, *RSC Med. Chem.*, 2023, **14**, 2438–2459.
10 S. J. Allison, J. Bryk, C. J. Clemett, R. A. Faulkner, M. Ginger, H. B. S. Griffiths, J. Harmer, P. J. Owen-Lynch, E. Pinder, H. Wurdak, R. M. Phillips and C. R. Rice, *Nat. Commun.*, 2021, **12**, 3898–3913.
11 M. J. Hannon, V. Moreno, M. J. Prieto, E. Moldrheim, E. Sletten, I. Meistermann, C. J. Isaac, K. J. Sanders and A. Rodger, *Angew. Chem., Int. Ed.*, 2001, **40**, 880–884.
12 A. D. Richards, A. Rodger, M. J. Hannon and A. Bolhuis, *Int. J. Antimicrob. Agents*, 2009, **33**, 469–472.
13 V. Brabec, S. E. Howson, R. A. Kaner, R. M. Lord, J. Malina, R. M. Phillips, Q. M. A. Abdallah, P. C. McGowan, A. Rodger and P. Scott, *Chem. Sci.*, 2013, **4**, 4407–4416.
14 A. D. Faulkner, R. A. Kaner, Q. M. A. Abdallah, G. Clarkson, D. J. Fox, P. Gurnani, S. E. Howson, R. M. Phillips, D. I. Roper, D. H. Simpson and P. Scott, *Nat. Chem.*, 2014, **6**, 797–803.
15 S. J. Allison, D. Cooke, F. S. Davidson, P. I. P. Elliott, R. A. Faulkner, H. B. S. Griffiths, O. J. Harper, O. Hussain, P. J. Owen-Lynch, R. M. Phillips, C. R. Rice, S. L. Shepherd and R. T. Wheelhouse, *Angew. Chem.*, 2018, **130**, 9947–9952.

16 J. Han, A. Schmidt, T. Zhang, H. Permentier, G. M. M. Groothuis, R. Bischoff, F. E. Kühn, P. Horvatovich and A. Casini, *Chem. Commun.*, 2017, **53**, 1405–1408.
17 A. Adamski, M. A. Fik, M. Kubicki, Z. Hnatejko, D. Gurda, A. Fedoruk-Wyszomirska, E. Wyszko, D. Kruszka, Z. Dutkiewicz and V. Patroniak, *New J. Chem.*, 2016, **40**, 7943–7957.
18 M. A. Fik, A. Gorczyński, M. Kubicki, Z. Hnatejko, A. Fedoruk-Wyszomirska, E. Wyszko, M. Giel-Pietraszuk and V. Patroniak, *Eur. J. Med. Chem.*, 2014, **86**, 456–468.
19 A. Pöthig, S. Ahmed, H. C. Winther-Larsen, S. Guan, P. J. Altmann, J. Kudermann, A. M. S. Andresen, T. Gjøen and O. A. H. Åstrand, *Front. Chem.*, 2018, **6**, 584.
20 V. Venkatesh, M. D. B. Kumaran, R. K. Saravanan, P. T. Kalaichelvan and S. Verma, *ChemPlusChem*, 2016, **81**, 1266–1271.
21 R. A. S. Vasdev, D. Preston, S. Ø. Scottwell, H. J. L. Brooks, J. D. Crowley and M. P. Schramm, *Molecules*, 2016, **21**, 1548–1561.
22 S. E. Howson, A. Bolhuis, V. Brabec, G. J. Clarkson, J. Malina, A. Rodger and P. Scott, *Nat. Chem.*, 2012, **4**, 31–36.
23 M. G. Rippon and A. A. Rogers, *Wounds Int.*, 2025, **16**, 20–37.
24 L. Yang, D. R. Powell and R. P. Houser, *Dalton Trans.*, 2007, **9**, 955–964.
25 D. Rosiak, A. Okuniewski and J. Chojnacki, *Polyhedron*, 2018, **146**, 35–41.
26 C. Serrano-Nascimento and M. T. Nunes, *Front. Endocrinol.*, 2022, **13**, 995503.
27 W. K. Jung, H. C. Koo, K. W. Kim, S. Shin, S. H. Kim and Y. H. Park, *Appl. Environ. Microbiol.*, 2008, **74**, 2171–2178.
28 T. G. Meikle, B. P. Dyett, J. B. Strachan, J. White, C. J. Drummond and C. E. Conn, *Appl. Mater. Interfaces*, 2020, **12**, 6944–6954.
29 (*a*) CCDC 2516767: Experimental Crystal Structure Determination, 2026, DOI: 10.5517/ccdc.csd.cc2qgx15; (*b*) CCDC 2516768: Experimental Crystal Structure Determination, 2026, DOI: 10.5517/ccdc.csd.cc2qgx26.